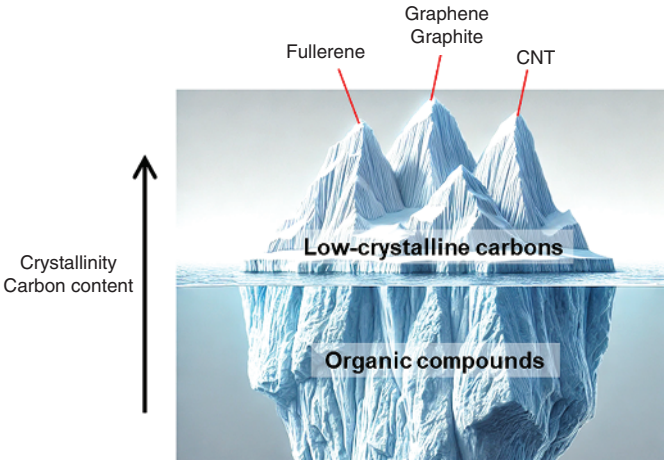

Figure 1.5 The "Iceberg Model" for carbon materials. The original illustration [57] has been adapted and stylized to fit the context of this book.

Despite the vast diversity of organic compounds, any precursor can ultimately yield carbon materials once the carbon content is sufficiently enriched. When the carbon concentration exceeds approximately 90%, the material is generally considered a carbon material (corresponding to the region above the water surface in the Iceberg Model). However, these materials exhibit a wide range of crystallinity, from low-crystalline to highly crystalline structures. Low-crystallinity carbon materials include charcoal, activated carbon, carbon fibers, carbon black, and glassy carbon. By increasing crystallinity through high-temperature treatment or catalytic processes, these materials can be further refined, eventually forming highly ordered structures such as fullerenes, CNTs, graphene, and graphite.

As illustrated by the 'Iceberg Model', there are countless pathways for synthesizing sp^2-carbon materials from organic compounds, reflecting the enormous diversity of organic precursors, and numerous methods have been proposed over the years. These synthesis routes can be broadly classified into solid-phase carbonization, liquid-phase carbonization, and gas-phase carbonization, depending on the physical state of the precursor during the transformation process. Thus, understanding the fundamental principles behind these carbonization mechanisms is crucial for developing effective sp^2-carbon synthesis strategies as it allows for precise control over the structures, crystallinity, and functional properties of the resulting materials.

1.2.1 Solid-Phase Carbonization

When pieces of wood or plants are pyrolyzed under oxygen-deficient conditions at high temperatures, they transform into charcoal, one of the earliest carbon materials used by humankind. Charcoal retains the original morphology of the wood precursor due to the 3D cross-linked structure of lignin, which, upon carbonization, forms an intricate network of interconnected graphene sheets. This process, where

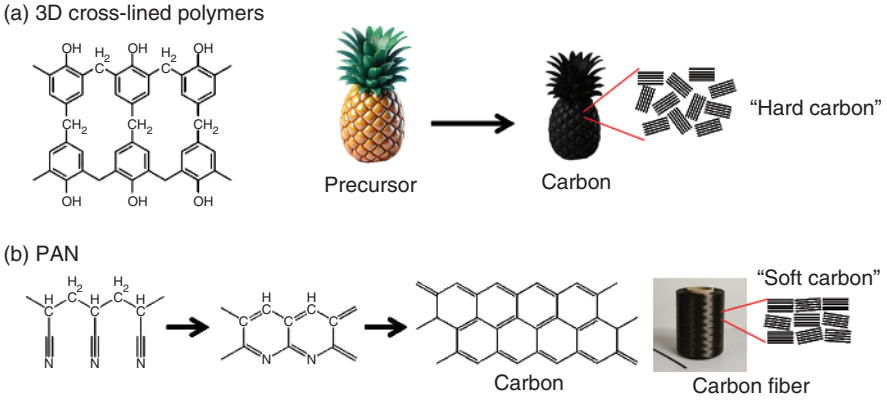

Figure 1.6 Schematic illustrations of solid-phase carbonization processes for (a) 3D cross-linked polymers and (b) polyacrylonitrile (PAN).

a solid precursor is converted into carbon while maintaining its shape, is known as solid-phase carbonization (Figure 1.6a). While the overall morphology is preserved, a slight volume shrinkage typically occurs. Similarly, thermosetting polymers, such as phenolic resins and furan resins, which possess 3D cross-linked networks, are widely used as precursors for carbon materials that retain their original shape *via* solid-phase carbonization. Carbon derived from these polymers consists of graphene sheets randomly arranged and often interlinked, making it difficult to convert into graphite even at temperatures exceeding 2,000 °C. This type of carbon is referred to as *hard carbon*, characterized by its high structural disorder and resistance to graphitization. Hard carbon is of significant importance as an anode material in lithium-ion and sodium-ion batteries, offering high capacity and structural stability [58].

In addition to resins with 3D cross-linking, polyacrylonitrile (PAN) is another widely used precursor for solid-phase carbonization, particularly in the production of carbon fibers (Figure 1.6b) and graphite sheets. Unlike lignin-based materials, PAN does not initially possess a 3D cross-linked structure, but during thermal decomposition, it undergoes structural transformation into graphene-like layers, making it a graphitizable carbon, commonly referred to as *soft carbon*. When PAN fibers are heat treated at high temperatures, they yield highly crystalline, high-strength carbon fibers, which are extensively used in aerospace, automotive, and high-performance composite applications.

1.2.2 Liquid-Phase Carbonization

When thermoplastic polymers, such as polyvinyl chloride or polyvinyl alcohol, are heated, they undergo thermal decomposition above 200 °C, transitioning into pitch, a complex mixture of polycyclic aromatic hydrocarbons (Figure 1.7). At around 300 °C, pitch remains in a liquid state, but as the temperature increases further, it solidifies, ultimately transforming into a sp^2-carbon material. This process, in which the precursor material passes through a liquid phase before carbonization, is

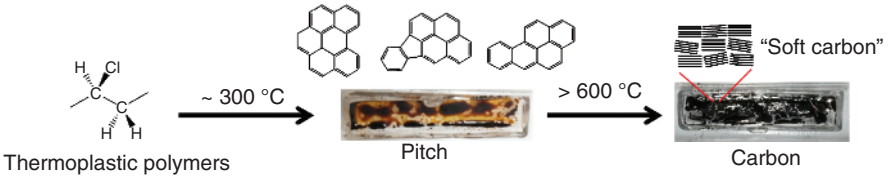

Figure 1.7 Schematic illustration of liquid-phase carbonization.

referred to as liquid-phase carbonization. The structural characteristics of the liquid precursor are largely retained in the final carbon material. Instead of synthesizing pitch *in situ*, coal tar pitch and similar materials can also be directly used as precursors. Because liquid carbon precursors can easily infiltrate the nanopores of template materials, such as oxide ceramics [59], templating techniques are commonly used to achieve precise control over the nanostructure of the resulting carbon materials. Specifically, mesoporous oxide ceramics and oxide ceramic nanoparticles are frequently used as templates to guide the formation of well-defined carbon nanostructures. Additionally, since polycyclic aromatic hydrocarbons in pitch exhibit a high degree of parallel alignment, the resulting carbon material tends to be soft carbon, which can be further processed to enhance its graphitic structure.

1.2.3 Gas-Phase Carbonization

Gas-phase carbonization refers to the thermal decomposition of gaseous carbon precursors, such as hydrocarbon gases and alcohols, at high temperatures, leading to the formation of carbon materials. This method is widely used in industrial production, particularly for carbon black. In the flame method (Figure 1.8a), hydrocarbon gases such as acetylene and vaporized liquid fuels are fed into a burner, where combustion generates soot, which consists of interconnected spherical carbon black nanoparticles. In the absence of catalysts, hydrocarbons decompose thermally, resulting in the formation of these nanocarbon aggregates. Fullerenes can also be synthesized using a similar flame-based approach.

In contrast, when carbon precursor gases are thermally decomposed without direct combustion, the process is referred to as chemical vapor deposition (CVD) (Figure 1.8b). Catalyst-free CVD, where a hydrocarbon source undergoes pyrolysis and deposits carbon onto a substrate, is used in the synthesis of highly oriented pyrolytic graphite (HOPG) and molecular sieving carbons. Meanwhile, catalyst-assisted CVD, using transition metals or oxide ceramics, enables the controlled synthesis of nanostructured carbon materials, such as CNTs and graphene. In particular, catalytic CVD with nanoporous oxide ceramic templates has emerged as a promising strategy for fabricating 3D graphene architectures with highly controlled nanostructures [60]. One of the close-to-genuine 3D graphene materials introduced in this book, graphene mesosponge [49], is synthesized using an oxide ceramic-catalyzed CVD process, enabling precise structural control and enhanced material properties.

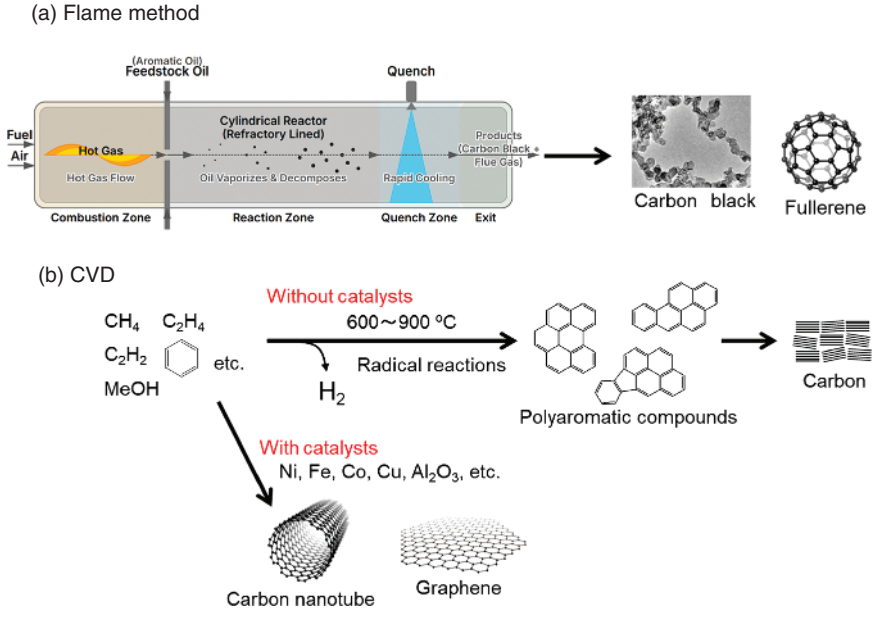

Figure 1.8 Schematic illustration of gas-phase carbonization. (a) Flame method. (b) Chemical vapor deposition (CVD).

References

1 Samara Carbon Allotrope Database (SACADA). https://www.sacada.info/ (accessed 12 January 2026).

2 Frondel, C. and Marvin, U.B. (1967). Lonsdaleite, a hexagonal polymorph of diamond. *Nature* 214: 587–589.

3 Bundy, F.P. and Kasper, J.S. (1967). Hexagonal diamond – a new form of carbon. *J. Chem. Phys.* 46: 3437–3446.

4 Sheng, X.-L., Yan, Q.-B., Ye, F. et al. (2011). T-carbon: a novel carbon allotrope. *Phys. Rev. Lett.* 106: 155703.

5 Ding, L., Stilwell, J., Zhang, T. et al. (2005). Molecular characterization of the cytotoxic mechanism of multiwall carbon nanotubes and nano-onions on human skin fibroblast. *Nano Lett.* 5: 2448–2464.

6 Hammel, E., Tang, X., Trampert, M. et al. (2004). Carbon nanofibers for composite applications. *Carbon* 42: 1153–1158.

7 Kroto, H.W., Heath, J.R., Obrien, S.C. et al. (1985). C_{60}: buckminsterfullerene. *Nature* 318: 162–163.

8 Ajie, H., Alvarez, M.M., Anz, S.J. et al. (1990). Characterization of the soluble all-carbon molecules C_{60} and C_{70}. *J. Phys. Chem.* 94: 8630–8633.

9 Maiti, A., Brabec, C.J., and Bernholc, J. (1993). Structure and energetics of single and multilayer fullerene cages. *Phys. Rev. Lett.* 70: 3023–3026.

10 Pech, D., Brunet, M., Durou, H. et al. (2010). Ultrahigh-power micrometre-sized supercapacitors based on onion-like carbon. *Nat. Nanotechnol.* 5: 651–654.

11 Iijima, S. and Ichihashi, T. (1993). Single-Shell carbon nanotubes of 1-nm diameter. *Nature* 363: 603–605.

12 Iijima, S. (1991). Helical microtubules of graphitic carbon. *Nature* 354: 56–58.

13 Saito, R., Dresselhaus, G., and Dresselhaus, M.S. (1996). Tunneling conductance of connected carbon nanotubes. *Phys. Rev. B* 53: 2044–2050.

14 Iijima, S., Brabec, C., Maiti, A., and Bernholc, J. (1996). Structural flexibility of carbon nanotubes. *J. Chem. Phys.* 104: 2089–2092.

15 Endo, M. and Kroto, H.W. (1992). Formation of carbon nanofibers. *J. Phys. Chem.* 96: 6941–6944.

16 Baker, R.T.K. (1989). Catalytic growth of carbon filaments. *Carbon* 27: 315–323.

17 González-Muñoz, D., Martín-Somer, A., Strobl, K. et al. (2021). Enhancing visible-light photocatalysis via endohedral functionalization of single-walled carbon nanotubes with organic dyes. *ACS Appl. Mater. Interfaces* 13: 24877–24886.

18 Nova-Fernández, J.L., González-Muñoz, D., Pascual-Coca, G. et al. (2024). Enhancing the photocatalytic activity via direct covalent functionalization in single-walled carbon nanotubes. *Adv. Funct. Mater.* 34: 13.

19 I. Jeon, Matsuo, Y., and Maruyama, S. (2018). Single-walled carbon nanotubes in solar cells. *Top. Curr. Chem.* 376: 28.

20 Muchuweni, E., Mombeshora, E.T., Martincigh, B.S., and Nyamori, V.O. (2022). Recent applications of carbon nanotubes in organic solar cells. *Front. Chem.* 9: 16.

21 Patel, K., Prochowicz, D., Akin, S. et al. (2023). Applications of carbon-based materials for improving the performance and stability of perovskite solar cells. *Energ. Technol.* 11: 28.

22 Islam, A.E. (2013). Variability and reliability of single-walled carbon nanotube field effect transistors. *Electronics* 2: 332–367.

23 Bishop, M.D., Hills, G., Srimani, T. et al. (2020). Fabrication of carbon nanotube field-effect transistors in commercial silicon manufacturing facilities. *Nat. Electron.* 3: 492–501.

24 Dewey, H.M., Lamb, A., and Budhathoki-Uprety, J. (2024). Recent advances on applications of single-walled carbon nanotubes as cutting-edge optical nanosensors for biosensing technologies. *Nanoscale* 16: 16344–16375.

25 Guo, S.Y., Hou, P.X., Zhang, F. et al. (2022). Gas sensors based on single-wall carbon nanotubes. *Molecules* 27: 22.

26 Shi, J.X., Lei, X.W., and Natsuki, T. (2021). Review on carbon nanomaterials-based nano-mass and nano-force sensors by theoretical analysis of vibration behavior. *Sensors* 21: 20.

27 Li, C.Y. and Chou, T.W. (2003). Single-walled carbon nanotubes as ultrahigh frequency nanomechanical resonators – art. no. 073405. *Phys. Rev. B* 68: 3.

28 Sirisinudomkit, P., Senokos, E., Rubio, N., and Shaffer, M.S.P. (2021). Reductive processing of single walled carbon nanotubes for high volumetric performance supercapacitors. *Mater. Adv.* 2: 1981–1992.

29 Zheng, Y.J., Dai, W.Y., Zhang, X.Q. et al. (2022). Nanotube-based heterostructures for electrochemistry: a mini-review on lithium storage, hydrogen evolution and beyond. *J. Energy Chem.* 70: 630–642.

30 Geim, A.K. and Novoselov, K.S. (2007). The rise of graphene. *Nat. Mater.* 6: 183–191.

31 Novoselov, K.S., Geim, A.K., Morozov, S.V. et al. (2004). Electric field effect in atomically thin carbon films. *Science* 306: 666–669.

32 Lee, C., Wei, X., Kysar, J.W., and Hone, J. (2008). Measurement of the elastic properties and intrinsic strength of monolayer graphene. *Science* 321: 385–388.

33 Bolotin, K.I., Sikes, K.J., Jiang, Z. et al. (2008). Ultrahigh electron mobility in suspended graphene. *Solid State Commun.* 146: 351–355.

34 Balandin, A.A., Ghosh, S., Bao, W. et al. (2008). Superior thermal conductivity of single-layer graphene. *Nano Lett.* 8: 902–907.

35 Nair, R.R., Blake, P., Grigorenko, A.N. et al. (2008). Fine structure constant defines visual transparency of graphene. *Science* 320: 1308–1308.

36 Nakada, K., Fujita, M., Dresselhaus, G., and Dresselhaus, M.S. (1996). Edge state in graphene ribbons: nanometer size effect and edge shape dependence. *Phys. Rev. B* 54: 17954–17961.

37 Son, Y.-W., Cohen, M.L., and Louie, S.G. (2006). Energy gaps in graphene nanoribbons. *Phys. Rev. Lett.* 97: 216803.

38 Trauzettel, B., Bulaev, D.V., Loss, D., and Burkard, G. (2007). Spin qubits in graphene quantum dots. *Nat. Phys.* 3: 192–196.

39 Ponomarenko, L.A., Schedin, F., Katsnelson, M.I. et al. (2008). Chaotic Dirac billiard in graphene quantum dots. *Science* 320: 356–358.

40 Berger, C., Song, Z., Li, X. et al. (2006). Electronic confinement and coherence in patterned epitaxial graphene. *Science* 312: 1191–1196.

41 Novoselov, K.S., McCann, E., Morozov, S.V. et al. (2006). Unconventional quantum Hall effect and Berry's phase of 2π in bilayer graphene. *Nat. Phys.* 2: 177–180.

42 Cao, Y., Fatemi, V., Fang, S. et al. (2018). Unconventional superconductivity in magic-angle graphene superlattices. *Nature* 556: 43–50.

43 Biscoe, J. and Warren, B.E. (1942). An X-ray study of carbon black. *J. Appl. Phys.* 13: 364–371.

44 Takaba, H., Omachi, H., Yamamoto, Y. et al. (2009). Selective synthesis of 12 cycloparaphenylene. *Angew. Chem.-Int. Ed.* 48: 6112–6116.

45 Yamago, S., Watanabe, Y., and Iwamoto, T. (2010). Synthesis of 8 cycloparaphenylene from a square-shaped tetranuclear platinum complex. *Angew. Chem.-Int. Ed.* 49: 757–759.

46 Kawasumi, K., Zhang, Q.Y., Segawa, Y. et al. (2013). A grossly warped nanographene and the consequences of multiple odd-membered-ring defects. *Nat. Chem.* 5: 739–744.

47 Mackay, A.L. and Terrones, H. (1991). Diamond from graphite. *Nature* 352: 762.

48 Lenosky, T., Gonze, X., Teter, M., and Elser, V. (1992). Energetics of negatively curved graphitic carbon. *Nature* 355: 333–335.

49 Nishihara, H., Simura, T., Kobayashi, S. et al. (2016). Oxidation-resistant and elastic mesoporous carbon with single-layer graphene walls. *Adv. Funct. Mater.* 26: 6418–6427.

50 Kudryavtsev, Y.P., Evsyukov, S.E., Guseva, M.B. et al. (1993). Carbyne – the third allotropic form of carbon. *Russ. Chem. Bull.* 42: 399–413.

51 Shi, L., Rohringer, P., Suenaga, K. et al. (2016). Confined linear carbon chains as a route to bulk carbyne. *Nat. Mater.* 15: 634–639.

52 Robertson, J. (1992). Properties of diamond-like carbon. *Surf. Coat. Technol.* 50: 185–203.

53 Vasudev, M.C., Anderson, K.D., Bunning, T.J. et al. (2013). Exploration of plasma-enhanced chemical vapor deposition as a method for thin-film fabrication with biological applications. *ACS Appl. Mater. Interfaces* 5: 3983–3994.

54 Tan, X., Li, J., Meng, K., and Zhai, H. (2023). Microstructures and visible-infrared optical properties of diamond-like carbon films deposited by magnetron sputtering. *Diam. Relat. Mater.* 133: 109724.

55 Li, Y., Xu, L., Liu, H., and Li, Y. (2014). Graphdiyne and graphyne: from theoretical predictions to practical construction. *Chem. Soc. Rev.* 43: 2572–2586.

56 Yue, Q., Chang, S., Kang, J. et al. (2013). Mechanical and electronic properties of graphyne and its family under elastic strain: theoretical predictions. *J. Phys. Chem. C* 117: 14804–14811.

57 Ohtani, S. (1997). *Tanso Jimon Jitou [in Japanese]*. Shoukabou.

58 LeGe, N., He, X.-X., Wang, Y.-X. et al. (2023). Reappraisal of hard carbon anodes for practical lithium/sodium-ion batteries from the perspective of full-cell matters. *Energy Environ. Sci.* 16: 5688–5720.

59 Orikasa, H., Akahane, T., Okada, M. et al. (2009). Electrochemical behavior of carbon nanorod arrays having different graphene orientations and crystallinity. *J. Mater. Chem.* 19: 4615–4621.

60 Nishihara, H. and Kyotani, T. (2012). Templated nanocarbons for energy storage. *Adv. Mater.* 24: 4473–4498.